BBA - Bioenergetics 1860 (2019) 148080

Contents lists available at ScienceDirect

BBA - Bioenergetics

journal homepage: www.elsevier.com/locate/bbabio

Characterization and X-ray structure of the NADH-dependent coenzyme A disulfide reductase from *Thermus thermophilus*☆

Andrea M. Lencina[a], Juergen Koepke[b], Julia Preu[b], Cornelia Muenke[b], Robert B. Gennis[a], Hartmut Michel[b,*], Lici A. Schurig-Briccio[a,*]

[a] Department of Biochemistry, University of Illinois, 600 S. Mathews Street, Urbana, IL 61801, USA
[b] Department of Molecular Membrane Biology, Max Planck Institute of Biophysics, Max-von-Laue-Str. 3, D-60438 Frankfurt am Main, Germany

ARTICLE INFO

Keywords:
Coenzyme A disulfide reductase
NADH oxidation
X-ray structure
Flavoprotein
Thermus thermophilus

ABSTRACT

The crystal structure of the enzyme previously characterized as a type-2 NADH:menaquinone oxidoreductase (NDH-2) from *Thermus thermophilus* has been solved at a resolution of 2.9 Å and revealed that this protein is, in fact, a coenzyme A-disulfide reductase (CoADR). Coenzyme A (CoASH) replaces glutathione as the major low molecular weight thiol in *Thermus thermophilus* and is maintained in the reduced state by this enzyme (CoADR). Although the enzyme does exhibit NADH:menadione oxidoreductase activity expected for NDH-2 enzymes, the specific activity with CoAD as an electron acceptor is about 5-fold higher than with menadione. Furthermore, the crystal structure contains coenzyme A covalently linked Cys44, a catalytic intermediate (Cys44-S-S-CoA) reduced by NADH via the FAD cofactor. Soaking the crystals with menadione shows that menadione can bind to a site near the redox active FAD, consistent with the observed NADH:menadione oxidoreductase activity. CoADRs from other species were also examined and shown to have measurable NADH:menadione oxidoreductase activity. Although a common feature of this family of enzymes, no biological relevance is proposed. The CoADR from *T. thermophilus* is a soluble homodimeric enzyme. Expression of the recombinant *Tt*CoADR at high levels in *E. coli* results in a small fraction that co-purifies with the membrane fraction, which was used previously to isolate the enzyme wrongly identified as a membrane-bound NDH-2. It is concluded that *T. thermophilus* does not contain an authentic NDH-2 component in its aerobic respiratory chain.

1. Introduction

Inside the cell, oxygen can be partially reduced by quinones, metal centers and flavin cofactors, leading to endogenous formation of reactive oxygen species (ROS), like superoxide ($O_2^{\cdot -}$), hydrogen peroxide (H_2O_2) and hydroxyl radical ($OH^{\cdot}$). These oxidant species can inactivate enzymes, as well as damage DNA and membrane lipids [1,2]. Thus, aerobic organisms need to maintain an intracellular reducing environment, while living in an oxidizing world. This is achieved by making use of different oxidoreductases, able to neutralize harmful species, and keeping high concentrations of low-molecular-weight (LMW) thiols, which serve as redox buffers, protecting the cell against a variety of stresses including ROS [3].

The best known LMW thiol is glutathione (GSH). However, GSH is not ubiquitous and is substituted in different species by high concentrations of other sulfur compounds such as bacillithiol (BSH), coenzyme A (CoA/CoASH), cysteine (Cys), ergothioneine (ESH) and mycothiol (MSH) [4,5]. In general, BSH is the major LMW thiol in firmicutes, GSH in eukaryotes and gram-negative bacteria, ESH in fungi and mycobacteria, and MSH in actinomycetes. Cys, a reactive amino acid, and CoASH, a universal metabolic cofactor, have important roles besides redox balance and are present in all organisms [6].

CoASH is an essential cofactor in numerous metabolic and energy-yielding reactions and is involved in the regulation of key metabolic enzymes [7]. CoASH is also the source of metabolic intermediates, which are required in several metabolic pathways, among them, fatty acid synthesis, the Krebs cycle and polyketide synthesis [8]. CoASH is resistant to autooxidation at high temperature, another advantage to its use as an antioxidant in thermophilic and hyperthermophilic organisms [9,10].

Thermus thermophilus is an aerobic thermophilic organism, with a maximum growth temperature of about 85 °C, originally isolated from a Japanese hot spring [11]. *T. thermophilus* lacks the ability to synthesize GSH but encodes the gene to synthetize CoASH and a gene that encodes

☆ CLASSIFICATION: Bioenergetics, Biochemistry, Redox Biology, Biological Sciences

* Corresponding authors.
E-mail addresses: Hartmut.Michel@biophys.mpg.de (H. Michel), lschurig@illinois.edu (L.A. Schurig-Briccio).

https://doi.org/10.1016/j.bbabio.2019.148080
Received 31 May 2019; Received in revised form 28 August 2019; Accepted 8 September 2019
Available online 11 September 2019
0005-2728/

for a putative CoA disulfide reductase (CoADR), suggesting that CoASH plays a role in redox homeostasis in this organism [12]. The gene predicted to encode *Tt*CoADR (NCBI gi: 46199786), has also been annotated as encoding an NADH oxidase [13], since both of these enzymes share a common set of sequence motifs. Cloning, expression and isolation of the protein encoded by this gene yielded a recombinant protein isolated from the membrane fraction of *E. coli* which was shown to have NADH:menaquinone oxidoreductase activity, expected for NDH-2 [14], an enzyme closely related to both CoADR and NADH oxidase [13]. The *T. thermophilus* NDH-2 (*Tt*NDH-2) was previously isolated and characterized from the membranes of *T. thermophilus* [15] with similar properties to the recombinant enzyme [14]. In the current work, the X-ray crystal structure of the recombinant enzyme thought to be *Tt*NDH-2 is reported and the enzyme is shown to actually be *Tt*CoADR. It is concluded that *T. thermophilus* does not contain an authentic NDH-2 component of its aerobic respiratory chain and that the previous identifications of *Tt*NDH-2, both from native membranes and a recombinant source [14,15], were based on enzyme activities that are artifacts and likely not physiologically meaningful.

2. Materials and methods

2.1. Strains and plasmids

E. coli and *T. thermophilus* strains expressing *Tt*CoADR were previously constructed by Venkatakrishnan et al. [14]. *E. coli* strains and plasmids expressing *B. anthracis* [16], *P. horikoshii* [17] and *S. aureus* [18] CoADR were constructed as previously described.

2.2. Cell growth, protein expression and purification and crystallization

Recombinant *E. coli* cells carrying the expression vectors encoding CoADRs were grown at 37 °C in LB medium, supplemented with the correspondent antibiotic, and induced with IPTG as described elsewhere [14,16,17,19]. *T. thermophilus* cells carrying the *Tt*CoADR into the shuttle vector pMKPbcbgaA were grown in Thermus Broth (TB) medium supplemented with 30 μg/ml kanamycin at 60 °C, as previously described [14].

Membrane and cytoplasmic fractions were obtained as follows. All procedures were performed at 4 °C. Briefly, cells were harvested and resuspended in buffer A (50 mM sodium phosphate buffer pH 7.5, 300 mM NaCl), plus 5 mM $MgSO_4$, DNAse I and protease inhibitor cocktail (Sigma-Aldrich Corp., St. Louis, MO, USA). They were then disrupted by passing three times through a microfluidizer at 80,000 psi pressure and the resulting extracts were centrifuged at 12,000 $\times g$ for 10 min to remove unbroken cells. Cell extracts were centrifuged once at 150,000 $\times g$ for 3 h to separate membrane fractions for further protein purification, or twice at 150,000 $\times g$ for 1 h to study the binding of different CoADRs to the membrane. When cell extracts were centrifuged twice, these were resuspended in buffer A in between centrifugation steps.

For protein purification, all steps were carried out at 4 °C. Membrane pellets were resuspended in buffer A plus the protease inhibitor cocktail and solubilized by addition of a stock solution of 20% dodecyl-β-D-maltoside (DDM) dropwise to a final concentration of 1%. The suspension was incubated at 4 °C for 2 h with mild agitation, then cleared by centrifugation at 65,000 $\times g$ for 1 h. Cytoplasmic supernatant and solubilized membranes were added to 5 ml of Ni-NTA resin (QIAGEN Sciences, Germantown, MD, USA) pre-equilibrated with buffer A plus 10 mM imidazole. The protein bound to the resin was washed with buffer A plus 50 mM imidazole (30 mM for *P. horikoshii* enzyme) and eluted with buffer A with 200 mM imidazole. Buffers used for purification from membrane fractions also contained 0.05% DDM. Eluates were concentrated by filtration, and imidazole was removed by a series of filtration and buffer A washing steps. The purified protein could be stored frozen at −80 °C after addition of glycerol to a final concentration of 10%.

For crystallization of the *T. thermophilus* enzyme the phosphate in buffer A was replaced by 20 mM HEPES (4-(2-hydroxyethyl)-1-piperazineethanesulfonic acid), pH 7.5, and a gel filtration step (Superdex 200 10/300, GE Healthcare Life Sciences, Freiburg, Germany) was added for final purification. For crystallization the protein was concentrated to 10 mg/ml using 20 mM HEPES-Na, pH 7.5, 0.3 M NaCl, 20 μM FAD and 0.02% (w/v) n-dodecyl-β-D-maltoside as buffer. Then 10% (v/v) glycerol and 100 nls of the well solution (0.8–1.4 M ammonium sulfate, 0.1 M ADA (2-[(2-amino-2-oxoethyl)-(carboxymethyl) amino]acetic acid Na, pH 6.4–6.8) were added to 100 nl aliquots for crystallization by vapor diffusion using our in-house crystallization facility [20]. Crystals appeared after 40 to 100 days. For freezing the crystals were transferred to the cryosolution (well solution containing 23.3% (v/v) glycerol) and flash frozen in a liquid nitrogen stream. Soaking with menadione was performed using a cryobuffer containing 21% (v/v) glycerol and 0.8 mM menadione (Sigma-Aldrich, Taufkirchen, Germany) for 100 min; for soaking with NADH the cryobuffer contained 42 mM NADH (Sigma-Aldrich) instead of menadione and the soaking time was reduced to 5 min prior to freezing.

2.3. Sequence and structure analysis

Sequence alignments were performed using CLUSTAL W [21]. Jalview software was used for visualization and analysis [22]. VMD software was used for structure visualization, analysis and comparison with existent X-ray structures [23].

2.4. Enzymatic activity assays

A UV–Vis spectrophotometer (Agilent Technologies, model 8453) was used to follow absorbance of NAD(P)H or 5,5′-dithiobis(2-nitrobenzoic acid) (DTNB) oxidation, after incubation of 2 nM enzyme for 2 min at 60 °C (or 42 °C as specified). All assays were carried out in 50 mM sodium phosphate buffer, pH 7.5 and 300 mM NaCl. Inhibition by p-chloromercuribenzoic acid (*p*-CMB) was tested by addition of 1 mM of the compound. NADH background oxidation was discounted when appropriate.

NAD(P)H:DTNB disulfide reductase: DTNB oxidation/TNB formation was detected by the increase in absorbance at 412 nm, in the presence of 100 μM of NAD(P)H and 2 mM of DTNB, as previously described [24].

NAD(P)H:CoAD reductase: NAD(P)H oxidation was determined by the decrease in absorbance at 340 nm, in the presence of 200 μM CoA disulfide (CoAD) and 100 μM NAD(P)H, as previously described [9].

NAD(P)H oxidase: NAD(P)H oxidation by oxygen was determined by the decrease in absorbance at 340 nm, in the presence of 100 μM NAD(P)H under aerobic conditions.

NAD(P)H peroxidase: NAD(P)H oxidation by H_2O_2 was determined by the decrease in absorbance at 340 nm, in the presence of 100 μM NAD(P)H and 200 μM H_2O_2 under aerobic conditions.

NAD(P)H:quinone reductase: NAD(P)H oxidation was determined by the decrease in absorbance at 340 nm, in the presence of 100 μM of the soluble quinone analog menadione (MD) and 100 μM NAD(P)H.

NADH oxidation coupled to E. coli respiratory chain: NAD(P)H oxidation was determined by the decrease in absorbance at 340 nm, in the presence of 125 μg/ml of *ΔnuoΔndh E. coli* membranes [25,26] and 100 μM NAD(P)H. Assays were performed at 42 °C to preserve membrane integrity.

2.5. Determination of kinetic parameters

The rate of NADH oxidation was determined using a UV–Vis spectrophotometer (Agilent Technologies, model 8453) by following absorbance at 340 nm upon addition of 2–200 μM NADH to the reaction mix containing 2–200 μM of CoAD and 2 nM enzyme, at 60 °C. Enzyme

rates are expressed as a turnover number (kcat) based on moles of NADH oxidized per second per mol of enzyme (mol NADH s^{-1} mol enzyme^{-1}).

2.6. Analytical methods

Protein purity was determined by SDS-PAGE using a 4–20% gradient gel (NuSep). The presence of recombinant his-tagged proteins was observed by western blot, using the Westernbreeze chromogenic kit (Thermo Fisher Scientific). Protein concentration in different cellular fractions was determined using the BCA kit (Thermo Fisher Scientific).

2.7. X-ray data collection, processing, and refinement

X-ray diffraction data were collected from the flash-frozen crystals using the synchrotron beamlines I03 at Diamond, UK and ID23-2 of the ESRF, France, respectively. The three collected data sets were indexed and processed with the program XDS [27] to a resolution of 2.9 or 3.0 Å, respectively. Because radiation damage was a severe problem several data collection runs were performed at different positions of the same crystal and the first 200, 150, or 50 undamaged reflections, respectively, where selected and combined in XSCALE to the used full datasets. Data collection statistics are listed in Table 1. F2mtz and cad from the CCP4 collection of crystallographic programs [28] were used to generate mtz-files for the next steps. For molecular replacement (MR), the PDB [29] entry 3nta [30] was selected as the best candidate using the Phyre2 web portal [31]. The final native structure had been determined employing the Phyre2 sequence corrected model of 3nta in the Phenix program Phaser-MR [32]. According to Matthews' coefficient [33] four copies of the molecule are necessary to fill the asymmetric unit (ASU). In a first run only one position for the protein molecule could be detected, while in a second run with the first found position fixed a second orientation readily appeared forming a dimer with the first one. Only with this dimer as new search ensemble further progress could be made, when in an additional MR run the orientation of a second dimer appeared. Thus, the four molecules inside the ASU are arranged in two dimers and were constrained in two non-crystallographic symmetry groups during refinement. Refinement of the four molecules against the three datasets was performed also in Phenix using its rigid body, torsion angle annealing, and individual adp protocols. Between the refinement rounds 2Fo–Fc electron density maps and Fo–Fc difference-density maps were inspected utilizing the graphics program Coot [34]. Some loop regions had to be improved and C- and N-terminal residues could be added. To detect firmly bound water molecules the find waters dialog of Coot was applied. Later during refinement some of the water positions could be replaced with atoms of the cofactors.

Table 1
Data collection statistics.

PDB IDs	6RUZ	6RVB	6RVH
Soaked with		50 mM NADH, 5 min	1 mM MD, 100 min
Data collection	Diamond	ESRF	Diamond
Wavelength (Å)	0.97625	0.8726	0.97625
Resolution (Å)	2.90	2.90	3.00
Unique reflections	72,881	75,111	63,717
Completeness (%) (last shell)	98.2 (99.3)	99.9(100.0)	95.0 (96.9)
I/σ_I (last shell)	5.58 (1.24)	7.31 (1.06)	4.37 (1.25)
R_{sym} (%) (last shell)	30.0 (212.9)	26.6 (204.7)	29.4 (134.4)
Redundancy	4.41	6.6	3.01
Space group	$P4_22_12$	$P4_22_12$	$P4_22_12$
Used positions	runs 1, 2, and 3	runs 4, 5, and 6	runs 1, 2, 3, and 4
Unit cell dimensions			
a, b, c (Å)	160.0, 160.0, 256.2	160.7, 160.7, 256.9	159.9, 159.9, 255.9
α, β, γ (°)	90, 90, 90	90, 90, 90	90, 90, 90
Refinement			
R_{work} (%)	20.69	20.08	21.49
R_{free} (%)	24.39	24.63	25.88
RMSD			
Bond length (Å)	0.034	0.032	0.034
Bond angle (°)	2.903	2.984	2.967
Number of molecules in ASU	4	4	4
B of cofactors (Å^2)		NAD[c]: 60	
	FAD[a]: 110 CoA[b]: 75	FAD: 80 CoA: 75	FAD: 80 CoA: 65 VK3[d]:100
B of protein molecules (Å^2)	71.79	53.71	53.13
Water molecules refined	66	112	136
Ramachandran plot			
Preferred (%)	87.02	87.19	85.94
Allowed (%)	7.94	7.77	8.16
Outliers (%)	5.05	5.05	5.90

[a] Flavin adenine dinucleotide.
[b] Coenzyme A.
[c] Nicotinamide adenine dinucleotide.
[d] Menadione.

3. Results

3.1. TtCoADR X-ray structure was determined at 2.9 Å resolution

The crystal structure of the *T. thermophilus* CoADR enzyme (PDB ID: 6RUZ), purified from *E. coli* after heterologous expression, was determined by molecular replacement based on *P. horikoshii* CoADR structure (PDB ID: 4FX9) [17]. *Tt*CoADR is a homodimer with a non-crystallographic 2-fold center of symmetry (Fig. 1). The fold is similar to that of other enzymes in the Flavin Disulfide Reductase (FDR) family, which includes NADH oxidases, NADH peroxidases and CoADR. The CoADR monomer consists of three domains, the FAD-binding domain, the NAD(P)H-binding domain and the C-terminal interface domain. The FAD- and NAD(P)H-binding domains of CoADR both have canonical Rossmann folds [35]. Specific details about the *Tt*CoADR structure compared to other CoADR are described below.

3.2. CoAD is the preferred electron acceptor for TtCoADR

Recombinant *Tt*CoADR was previously shown to have NADH:menaquinone oxidoreductase activity in vitro and designated an NDH-2 [14]. Its X-ray structure presented here, however, resembles a CoADR [9,10]. These inconsistent data are not surprising since many members of the FDR family are unable to be distinguished based only on their amino acid sequence. Consequently, many genes are misannotated and others are postulated to have particular functions without justification. Overlap of the NDH-2 structure from yeast (PDB ID: 4G73 and 4G74) with the *Tt*CoADR structure (PDB ID: 6RVH) shows that both enzymes have the same π-stacking of FAD and NADH head groups in the active site (Fig. 2). The menadione binding site identified in the structure of *Tt*CoADR is close to the analogous region that binds quinone in the structures of authentic NDH-2s [36]. The two C-terminal helices, α15 and α16, of authentic NDH-2 structures which are the membrane-binding regions, however, are missing in *Tt*CoADR.

The crystal structure of *Tt*CoADR contains a CoA molecule covalently bound to Cys44, close to the FAD and NADH molecules (Fig. 3). This cysteine corresponds to the conserved catalytic residue present in all group 3 FDR enzymes [37], typically within an SFXXC sequence motif, but which is SYXXC in *Tt*CoADR.

To understand the specificity of the enzyme for different substrates, activity assays were performed in the presence of NDH-2 and CoADR specific substrates: NADH/menadione (MD) and NADH/CoAD, respectively. In addition, the following substrates used by group 3 FDR

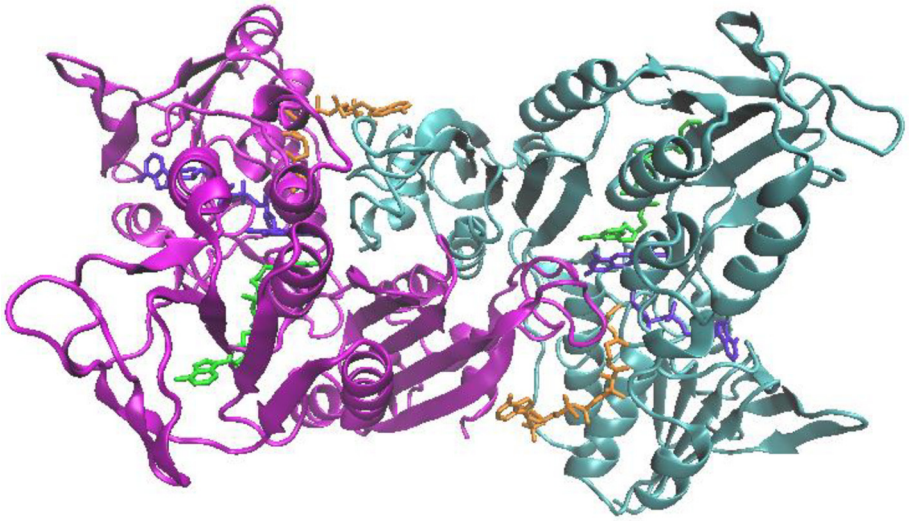

Fig. 1. Global fold of *Thermus thermophilus* CoADR. Structure (ribbon representation) of the CoADR dimer, colored by subunit: chain A, magenta; chain B, cyan. NADH (green), CoAD (orange) and FAD (purple) are represented as sticks in each monomer.

enzymes were examined in combination with NADH: DTNB, a synthetic disulfide substrate that can be reduced by CoADRs; H_2O_2, reduced by NADH peroxidases; and O_2, reduced by NADH oxidases (Table 2). It is worth noting that whereas the addition of 30 μM FAD increases the NADH:menadione reductase activity [14], as observed for other flavoproteins purified with suboptimal amounts of FAD per protein [26,38], the extra flavin does not affect the disulfide reductase activity of the enzyme.

NADH oxidation in the presence of CoAD is about 5-fold higher than the quinone reductase activity observed with menadione (k_{cat} is 1 NADH oxidized per second) (Table 2). DTNB is also reduced by *Tt*CoADR at a faster rate than menadione [17,39]. No disulfide reductase activity (DTNB) is seen after addition of the thiol-reactive compound *p*-CMB, which blocks the catalytic cysteine. *Tt*CoADR also shows low NADH-dependent oxidase and peroxidase activities at 60 °C, corresponding to 30% to 40% of the rate of menadione reduction. Oxidase, peroxidase and menadione reductase activities were not influenced by the presence of *p*-CMB, suggesting the cysteine residue is not involved in these reactions.

Although lacking transmembrane spans, NDH-2s are membrane-bound enzymes, able to reduce quinones present in the membrane bilayer. Since the in vitro rate of reduction of quinone by *Tt*CoADR (with NADH) is significantly higher than the rate of reduction of oxygen or peroxide, enzyme activity was also assayed in the presence of NADH plus *E. coli* membranes to test for coupling of NADH oxidation to the respiratory chain. Isolated membranes of an *E. coli* strain lacking membrane-associated NADH dehydrogenase activity (deficient in *Ec*NDH-2 and *Ec*Complex I) was used for these assays in order to remove any background NADH oxidation. No NADH oxidation was observed by purified *Tt*CoADR in the presence of these membranes, suggesting the quinone reductase activity is not relevant in vivo.

Table 3 summarizes steady state kinetics parameters K_m can k_{cat} for

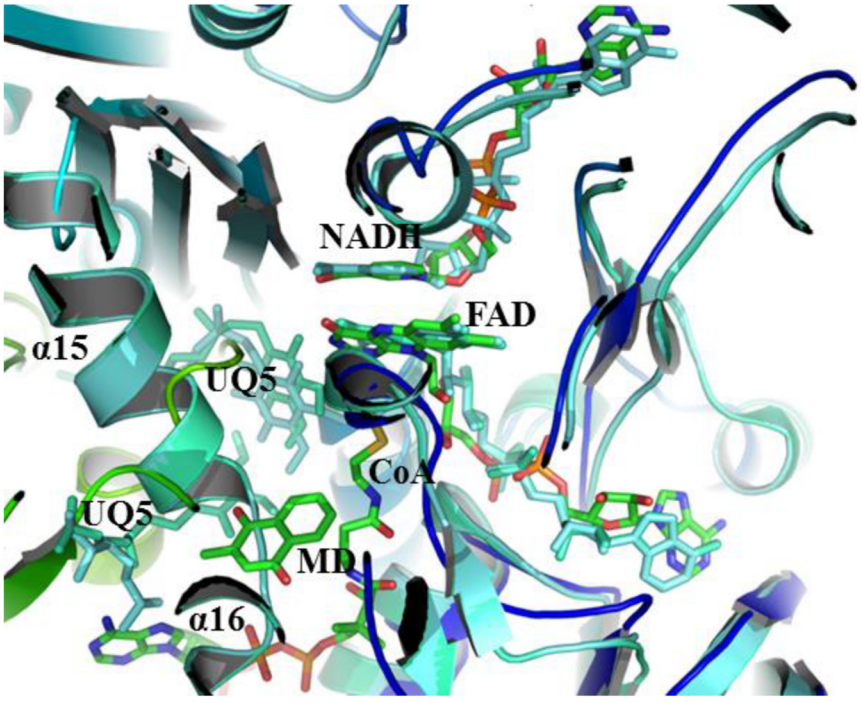

Fig. 2. Overlap of *Tt*CoADR soaked with 1 mM menadione and yeast NDH-2 (4G73 and 4G74) monomeric structures. Structures show similar fold but with different alignments in the dimer. Yeast NDH-2 is missing the CoAD molecule. The two NDH-2 structures are colored in sky blue and light green, respectively, while the two subunits of *Tt*CoADR shown here are colored in green and dark blue. The cofactors of *Tt*CoADR are drawn in ball and stick representation and color coded according to their atom type, while the prosthetic groups of NDH-2 are colored like their respective main chains.

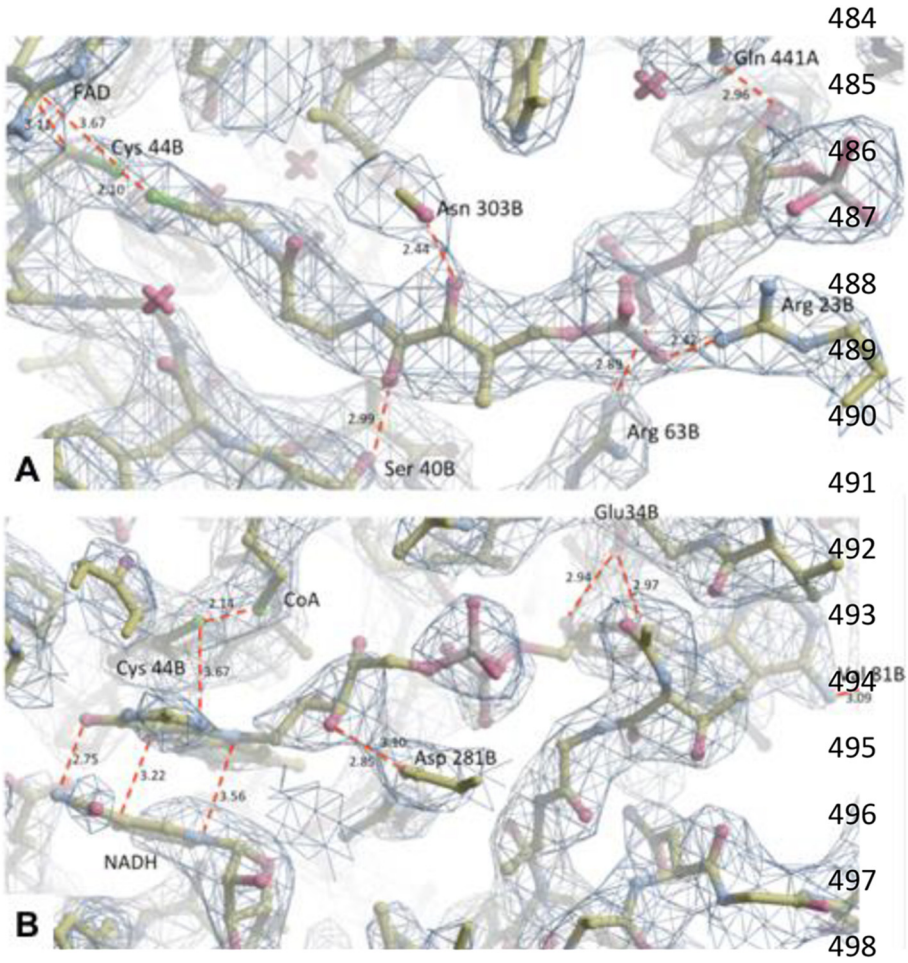

Fig. 3. CoASH binding site. (A) CoASH is found covalently bound to Cys44 at the active site upon purification. (B) The FAD group interacts with NADH through π-stacking, indicated by the three close distances of 2.75, 3.22, and 3.56 Å, respectively, and is aligned with the Cys44-S-S-CoA disulfide bond, favoring electron transfer. Dashed red lines indicate the distance in Å between the atoms at its end, which were found to be in close contact. The refined structure is given in ball and stick representation with the atoms colored according to their type. The electron density is given as a light blue mesh. Capital letters behind the residue numbers indicate the corresponding subunit.

Table 2
*Tt*CoADR enzyme activity with different electron acceptor substrates at 60 °C.

Substrate	[a]k_{cat} [s^{-1}]
Menadione	1.0 ± 0.1
[b]DTNB	1.5 ± 0.2
CoAD	5.5 ± 0.7
O_2	0.3 ± 0.0
H_2O_2	0.4 ± 0.1

[a]Activity is expressed as μmoles of NADH oxidized or [b]DTNB reduced per second at 60 °C. Data are expressed as average ± SD of three independent experiments.

the *Tt*CoADR and compares these values with those reported for CoADRs from other species. The data show that the kinetics parameters for *Tt*CoADR are in the same range as those of other CoADRs.

A structural comparation of the CoAD binding sites of the *Tt*CoADR, *Sa*CoADR and *Ph*CoADR shows (Fig. 4) that the CoAD binding site in *Tt*CoADR is more similar (size and topology) to the one in *Sa*CoADR than to the CoAD binding site in *Ph*CoADR. This is consistent with *Tt*CoADR and *Ph*CoADR using the same substrate (CoAD), whereas *Ph*CoADR uses persulfide and polysulfide derivatives of small thiols [17,40].

3.3. *TtCoADR exclusively oxidizes NADH*

CoADRs catalyze reduction of CoAD via oxidation of NAD(P)H. So far, there are several characterized CoADRs: the NADPH-dependent CoADRs from *S. aureus* and *P. horikoshii*; the CoADR from *B. anthracis* with dual-specificity for NADH/NADPH [8,10,12]; and the NADH-

Table 3
Steady state kinetics parameters for CoADRs from several species.

Source organism	Preferred substrate	K_m(NAD(P)H) [μM]	K_m(CoAD) [μM]	k_{cat} [s^{-1}]	k_{cat}/Km [$M^{-1}\,s^{-1}$]	Reference
P. horikoshii	NADPH	9–73	30	7–8	2×10^5	[9]
B. burgdorferi	NADH	nd	nd	14	nd	[41]
T. thermophilus[a]	NADH	2.5	72	5	7×10^4	This work
S. aureus	NADPH	1	3	27	9×10^6	[43]
B. anthracis	NAD(P)H	1–3	1	27–28	3×10^7	[16]

nd: Not determined.
[a] *T. thermophilus* K_m (NADH) = 2.5 ± 0.3; K_m (CoAD) = 71.6 ± 11.1; k_{cat} = 5.53 ± 0.68 s^{-1}. Data are expressed as average ± SD of three independent experiments.

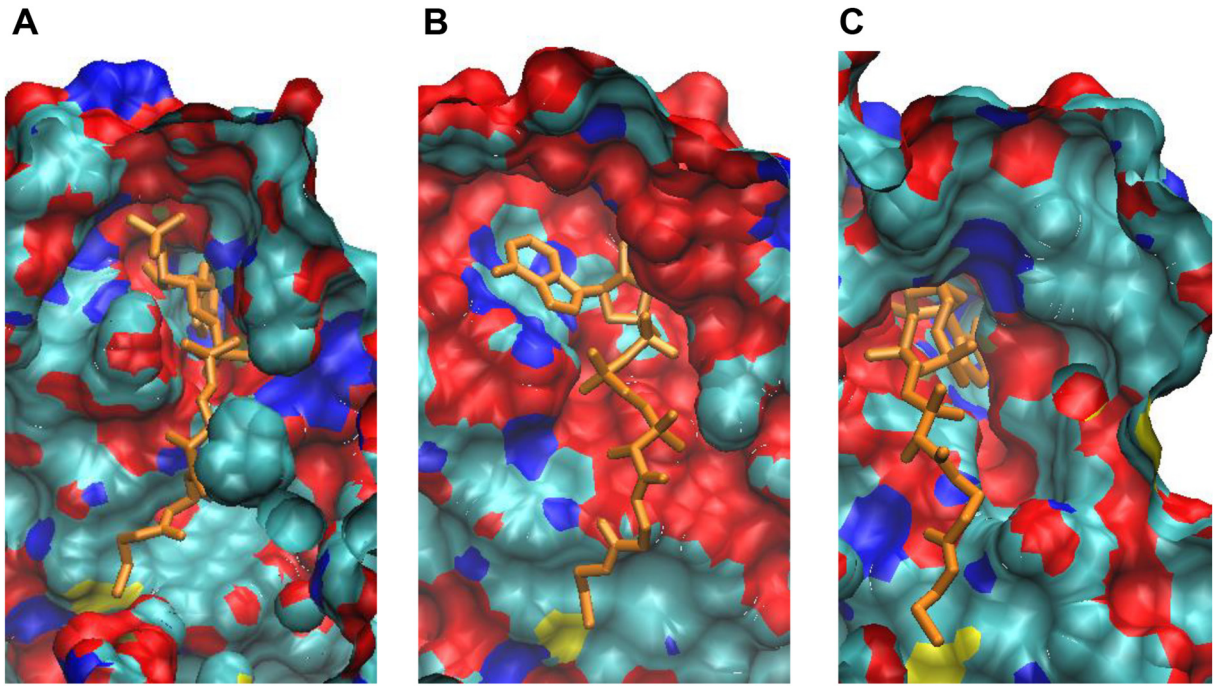

Fig. 4. Electrostatic surface maps of the (A) *Tt*CoADR, (B) SaCoADR (1YQZ) and (C) *Ph*CoADR (4FX9) CoA binding clefts. CoA is shown in orange sticks.

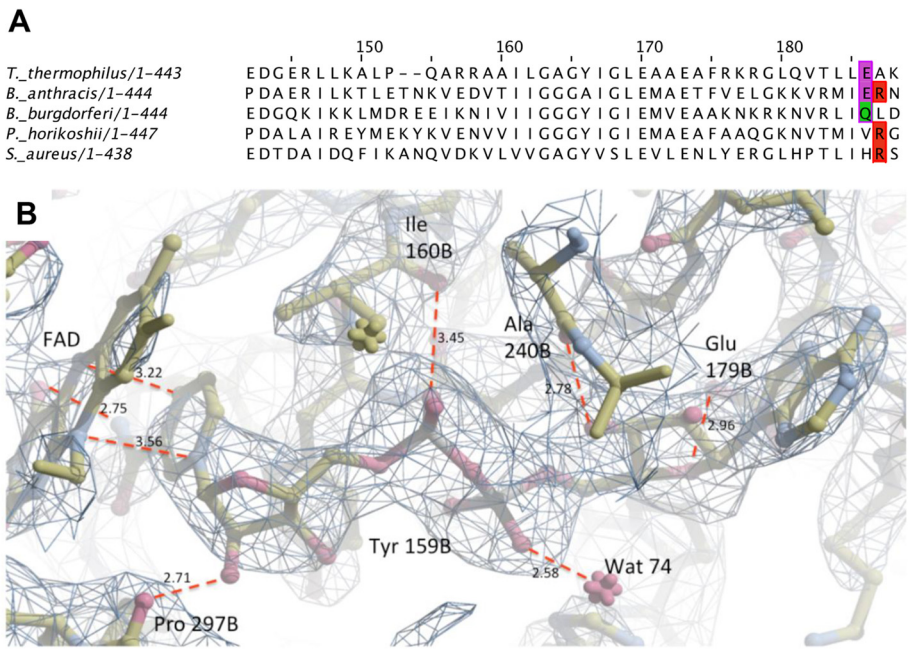

Fig. 5. *Tt*CoADR shows specificity for NADH. (A) *T. thermophilus* enzyme is predicted to only use NADH as a substrate, based on sequence alignments showing the presence of residues for specific interaction with NADH (magenta/green) and absence of those specific for NADPH (red) [16]. (B) NADH mainly interacts with FAD through π-stacking and hydrogen bonds to few amino acid residues, including Glu179. Representation of the refined structure and its electron density like in Fig. 3.

dependent enzyme from *B. burgdorferi* [41]. However, there is no structure available for this last one.

Specificity towards NADH or NADPH can be predicted based on conserved amino acids [16,42]. The most commonly described residues are a glutamate that interacts with the 2′-oxygen of the adenosine ribose in NADH, and an arginine that stabilizes the 2′-phosphate of the adenosine in NADPH. Sequence alignments of *Tt*CoADR with other CoADRs of known specificity predict NADH specificity for *Tt*CoARD by the presence of a glutamate in the position 179 and the absence of an arginine residue, which is replaced by Ala180 (Fig. 5A).

Soaking of the crystals with NADH allowed for structure determination of the NADH-bound structure (PDB ID: 6RVB). In this structure, the nicotinamide ring of NADH and the FAD isoalloxazine ring can be seen interacting primarily through π-stacking with only a few protein residues making close connections with NADH. Specifically, Glu179 can be seen in close contact with the adenosine ribose (Fig. 5B). These data are consistent with the lack of any catalytic function of *Tt*CoADR using NADPH as reductant, and identifies *Tt*CoADR as the first structure of a NADH-specific CoADR.

3.4. Other CoADRs can be found in the membrane fraction

Since *Tt*CoADR was initially reported by Yagi et al. [15], to have been purified from the membrane fraction, we initially isolated the protein from this fraction [14]. Although we demonstrate in the current work that the majority of the protein is in the cytosol, there is a small

Table 4
Distribution of CoADR in the cell in different organisms.

Organism	Cytoplasm:membrane	Total amount of CoADR (mg/l)[c]
B. anthracis	14:1	0.5
P. horikoshii	2:1	1.9
S. aureus[a]	95:1	57
T. thermophilus	95:1	6.4
T. thermophilus[b]	15:1	0.1

[a] *S. aureus* with no tag, overexpressed in *E. coli* BL21.
[b] *T. thermophilus* enzyme expressed in the native organism.
[c] mg of protein purified per liter of culture from cytoplasm and membrane combined.

fraction of the enzyme that remains membrane-bound in our protocols. To determine if the membrane-bound fraction is meaningful, the fraction of recombinant CoADR that was associated with the membrane fraction after two steps of washing and high speed centrifugation was determined for CoADR from different species. Data are summarized in Table 4, which shows the ratio of the amount of recombinant CoADR in the cytoplasmic and membrane fractions following cell disruption. Also shown is the total amount of CoADR per liter in the growth culture. Relatively small amounts of recombinant CoADR from each species sedimented with the membrane fraction. For *Tt*CoADR expressed in *E. coli*, overexpression produced 6.4 mg/l of protein and only 1% is found in the membrane fraction. Overexpression using *T. thermophilus* as the host resulted in a much lower protein yield (0.1 mg/l) with about 6% found in the membrane. Overproduction of the *S. aureus* CoADR is very high (57 mg/l) but only about 1% is found in the membrane fraction. Since we found no evidence of redox coupling between CoADR and the *E. coli* respiratory chain components, these minor amounts apparently associated with the membrane are interpreted as an artifact. An interesting case is the CoADR from the hyperthermophile *P. horikoshii*, where 33% of the protein sedimented with the membrane fraction. This was not further explored but is also likely not physiological meaningful.

3.5. Quinones can interact with CoADR at the CoAD binding site

*Tt*CoADR shows NADH oxidation in the presence of menadione, a soluble naphthoquinone that is an analogue of menaquinones. To determine where menadione binds, the protein structure was analyzed after soaking the crystals with menadione.

The soaked crystals, show a weak electron density for the menadione molecule, with a putative binding pocket at the dimer interface (Fig. 6A) with the two quinone oxygen atoms most clearly identified. The naphthoquinone ring is close to the disulfide bridge between the catalytic Cys44 and CoA (Fig. 6B). Hence, menadione binds to the enzyme at a position allowing direct electron transfer from the $FADH_2$ cofactor. Since *p*-CMB does not inhibit electron transfer to menadione, direct reduction from $FADH_2$ seems likely.

S. aureus CoADR has been crystallized in the presence of several CoAS-mimetics, which irreversibly bind and inhibit the catalytic cysteine [43]. A CoASH analogue containing a phenyl vinyl sulfone group (PhVS-CoA) shows the phenyl ring at the same site as the naphthoquinone ring in *Tt*CoADR when structures are superimposed (Fig. 7). During catalysis, CoAD is broken down into two CoAS molecules upon reduction: CoAS-I, which initially remains bound to the active cysteine, and CoAS-II, which dissociates from the enzyme. The electron-withdrawing group (Ph-VS) seen at the proposed CoAS-II site coincides with the CoAD binding cleft and overlaps with the bound menadione.

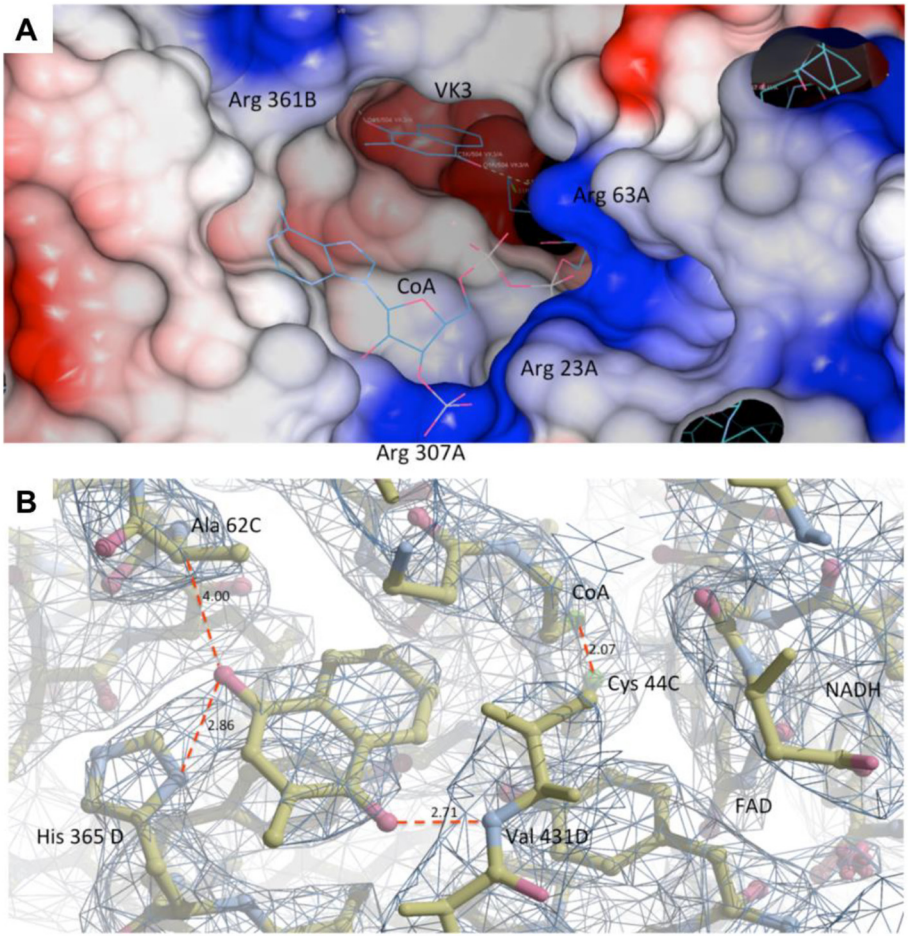

Fig. 6. Menadione binds at the dimer interface in close vicinity to the active site. (A) Menadione interacts with the enzyme at the interface of the dimer. (B) Amino acids from both monomers can be seen interacting with menadione at the binding pocket. The subunits shown here are indicated by the capital letters C and D after each residue numbers. Like in Figs. 3 and 5B, the electron density is shown as a light blue mesh while the atoms are color coded according to their atom type. Atoms in close contact are again connected by dashed red lines with their distance given in Å.

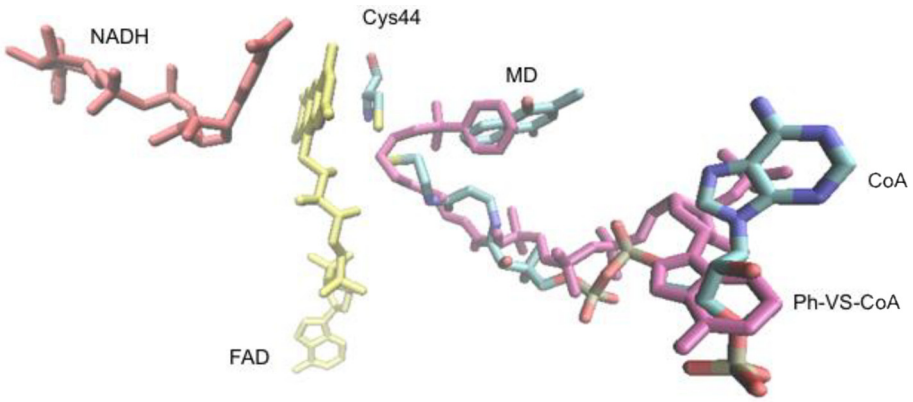

Fig. 7. Menadione binds at the CoAD binding cleft. *S. aureus* CoADR structure with the Ph-VS-CoA inhibitor bound is superimposed to the structure of the *Tt*CoADR with MD bound. The naphtoquinone ring from menadione (MD) reaches the active site of *Tt*CoADR through the CoAD binding cleft, binding at the putative CoAS-II site described in *S. aureus*, which is occupied by the phenyl group.

4. Discussion

4.1. T. thermophilus NDH-2 is a CoADR

CoADR is a group-3 FDR with a single redox-active Cys, part of a SFXXC motif, that reduces CoAD via formation of a protein-S-S-CoA mixed disulfide [37]. This group of FDRs also includes NADH oxidase and NADH peroxidase enzymes. NAD(P)H-dependent CoADRs have been isolated and characterized from the pathogenic firmicutes *S. aureus* [19,44] and *B. anthracis* [16], the Lyme disease spirochete *Borrelia burgdorferi* [41], and the thermophilic anaerobic archaeon *P. horikoshii* [9]. To this list, the current work adds the CoADR from *T. thermophilus*.

The initial goal of the project was to identify the gene encoding *T. thermophilus* NDH-2, a homodimeric, membrane-bound respiratory enzyme isolated and characterized by Yagi et al. [15], who first isolated *Tt*NDH-2 from membranes of the native organism. In an effort to identify the gene encoding for the enzyme reported by Yagi et al. [14], Venkatakrishnan et al. [15] cloned the gene NCBI gi:46199786 from *T. thermophilus* HB27 and purified the membrane-associated recombinant protein from an *E. coli* expression system. Although the recombinant enzyme was annotated as encoding an NADH oxidase, the isolated protein has very little NADH:O_2 oxidoreductase activity. In contrast, the isolated protein was found to oxidize NADH in the presence of a variety of quinone substrates, including menadione, and the NADH:menadione oxidoreductase specific activity is similar to that reported for the previously isolated *Tt*NDH-2 [14].

The current work clearly shows that the protein encoded by NCBI gi:46199786 is neither an NADH oxidase nor an NDH-2 but is, rather a CoADR. Furthermore, it is concluded that the genome of *T. thermophilus* HB27 does not encode an authentic NDH-2. The initial identification of *Tt*NDH-2 by Yagi et al. [15] was found to be a dihydrolipoyl dehydrogenase after mass spectrometry analyses (Takao Yagi, personal communication, unpublished data). This protein corresponds to the E3 subunit of the pyruvate dehydrogenase complex (among other 2-oxoacid decarboxylases), a soluble complex able to oxidize NADH and reduce dihydrolipoic acid to lipoic acid [45]. Hence, *Tt*NDH-2 has been incorrectly identified twice due in large part to the ability of the *Tt*CoADR as well as the E3 subunit of pyruvate dehydrogenase to catalyze the reduction of menadione by NADH. Since the enzyme assays are performed at temperatures well below the growth optimum for *T. thermophilus*, it is expected that specific activity values might be low, as is the case (Table 3). NADH:menadione oxidoreductase activity was also examined with other CoADRs (*Ph*CoADR and *Ba*CoADR) and shown to have one tenth of the measured CoADR activity for each enzyme. In the current work, the menadione binding site is located in the crystal structure, bound to the cleft in the enzyme where part of the CoA dimer binds, showing the origin of the artifactual menadione reductase activity.

One important property of NDH-2 enzymes is that they are membrane-bound and are monotopically bound to the cell membrane [36,46,47]. In contrast, CoADRs are soluble proteins. Here, it was demonstrated that when overexpressed in *E. coli*, a small amount of recombinant CoADRs from different sources co-sediment with the membrane fraction, even following washing the membranes and resedimentation. Adding to the possible confusion is the fact that a significant portion of recombinant NDH-2s, when overexpressed in *E. coli*, is found in the cytosolic fraction [26]. This is likely to be not physiologically relevant but has contributed to the incorrect identification of *Tt*CoADR as an NDH-2.

It appears that all reports of NDH-2 activity associated with the membranes of aerobically grown *T. thermophilus* are based on side reactions catalyzed by enzymes other than NDH-2. It is concluded that *T. thermophilus* does not contain an authentic NDH-2 and, therefore, must rely solely on Complex I to oxidize NADH and feed electrons into the aerobic respiratory chain.

Transparency document

The Transparency document associated with this article can be found, in online version.

Acknowledgments

We thank all members of the Gennis and Michel laboratories for help and useful discussions. We thank Dr. Claiborne (Wake Forest School of Medicine) for kindly providing the *E. coli* strain and plasmid expressing the CoADR from *B. anthracis* and for insightful scientific discussions and expertise. We also thank to Dr. Yagi (Scripps Research Institute, La Jolla) for providing us experimental information. We thank to Dr. Parsonage (Wake Forest School of Medicine) and Dr. Crane (Pomona College) for providing the *E. coli* strains and plasmids expressing the CoADRs from *P. horikoshii* and *S. aureus*, respectively. We thank Dr. G.N. Bennett (Rice University, Houston) for the GNB10608 strain. This work was supported by grants from the United States National Institutes of Health GM095600 and HL16101 to R.B.G. and from the Max Planck Society and the Deutsche Forschungsgemeinschaft (Cluster of Excellence “Macromolecular Complexes” Frankfurt) to H.M.

References

[1] J.A. Imlay, The molecular mechanisms and physiological consequences of oxidative stress: lessons from a model bacterium, Nat. Rev. Microbiol. 11 (2013) 443–454.
[2] B. Ezraty, A. Gennaris, F. Barras, J.F. Collet, Oxidative stress, protein damage and repair in bacteria, Nat. Rev. Microbiol. 15 (2017) 385–396.
[3] G. Roos, J. Messens, Protein sulfenic acid formation: from cellular damage to redox regulation, Free Radic. Biol. Med. 51 (2011) 314–326.
[4] K. Van Laer, C.J. Hamilton, J. Messens, Low-molecular-weight thiols in thiol-disulfide exchange, Antioxid. Redox Signal. 18 (2013) 1642–1653.
[5] R.C. Fahey, Glutathione analogs in prokaryotes, Biochim. Biophys. Acta 1830 (2013) 3182–3198.

[6] K. Van Laer, L. Buts, N. Foloppe, D. Vertommen, K. Van Belle, K. Wahni, G. Roos, L. Nilsson, L.M. Mateos, M. Rawat, N.A. van Nuland, J. Messens, Mycoredoxin-1 is one of the missing links in the oxidative stress defence mechanism of Mycobacteria, Mol. Microbiol. 86 (2012) 787–804.

[7] Abiko, Y. (1975) Metabolism of coenzyme A, Pp 1–25 in D M Greenberg, ed Metabolism of Sulphur Compounds. Academic Press, New York.

[8] H. Kleinkauf, The role of 4′-phosphopantetheine in t' biosynthesis of fatty acids, polyketides and peptides, BioFactors. 11 (2000) 91–92.

[9] D.R. Harris, D.E. Ward, J.M. Feasel, K.M. Lancaster, R.D. Murphy, T.C. Mallet, E.J. Crane 3rd, Discovery and characterization of a Coenzyme A disulfide reductase from Pyrococcus horikoshii. Implications for this disulfide metabolism of anaerobic hyperthermophiles, FEBS J. 272 (2005) 1189–1200.

[10] C.S. Hummel, K.M. Lancaster, E.J. Crane 3rd, Determination of coenzyme A levels in Pyrococcus furiosus and other Archaea: implications for a general role for coenzyme A in thermophiles, FEMS Microbiol. Lett. 252 (2005) 229–234.

[11] Oshima, T. I., K. (1974) Description of Thermus thermophilus (Yoshida and Oshima) comb. nov., a Nonsporulating Thermophilic Bacterium from a Japanese Thermal Spa, International Journal of Systematic and Evolutionary Microbiology 102–112.

[12] N.I. Nicely, D. Parsonage, C. Paige, G.L. Newton, R.C. Fahey, R. Leonardi, S. Jackowski, T.C. Mallett, A. Claiborne, Structure of the type III pantothenate kinase from Bacillus anthracis at 2.0 A resolution: implications for coenzyme A-dependent redox biology, Biochemistry. 46 (2007) 3234–3245.

[13] B.C. Marreiros, F.V. Sena, F.M. Sousa, A.P. Batista, M.M. Pereira, Type II NADH:quinone oxidoreductase family: phylogenetic distribution, structural diversity and evolutionary divergences, Environ. Microbiol. 18 (2016) 4697–4709.

[14] P. Venkatakrishnan, A.M. Lencina, L.A. Schurig-Briccio, R.B. Gennis, Alternate pathways for NADH oxidation in Thermus thermophilus using type 2 NADH dehydrogenases, Biol. Chem. 394 (2013) 667–676.

[15] T. Yagi, K. Hon-nami, T. Ohnishi, Purification and characterization of two types of NADH-quinone reductase from Thermus thermophilus HB-8, Biochemistry. 27 (1988) 2008–2013.

[16] J.R. Wallen, C. Paige, T.C. Mallett, P.A. Karplus, A. Claiborne, Pyridine nucleotide complexes with Bacillus anthracis coenzyme A-disulfide reductase: a structural analysis of dual NAD(P)H specificity, Biochemistry. 47 (2008) 5182–5193.

[17] S. Herwald, A.Y. Liu, B.E. Zhu, K.W. Sea, K.M. Lopez, M.H. Sazinsky, E.J. Crane 3rd, Structure and substrate specificity of the pyrococcal coenzyme A disulfide reductases/polysulfide reductases (CoADR/Psr): implications for S(0)-based respiration and a sulfur-dependent antioxidant system in Pyrococcus, Biochemistry. 52 (2013) 2764–2773.

[18] J. Luba, V. Charrier, A. Claiborne, Coenzyme A-disulfide reductase from Staphylococcus aureus: evidence for asymmetric behavior on interaction with pyridine nucleotides, Biochemistry. 38 (1999) 2725–2737.

[19] S.B. delCardayre, J.E. Davies, Staphylococcus aureus coenzyme A disulfide reductase, a new subfamily of pyridine nucleotide-disulfide oxidoreductase. Sequence, expression, and analysis of cdr, J. Biol. Chem. 273 (1998) 5752–5757.

[20] Y. Thielmann, J. Koepke, H. Michel, The ESFRI Instruct Core Centre Frankfurt: automated high-throughput crystallization suited for membrane proteins and more, J. Struct. Funct. Genom. 13 (2012) 63–69.

[21] J.D. Thompson, D.G. Higgins, T.J. Gibson, CLUSTAL W: improving the sensitivity of progressive multiple sequence alignment through sequence weighting, position-specific gap penalties and weight matrix choice, Nucleic Acids Res. 22 (1994) 4673–4680.

[22] A.M. Waterhouse, J.B. Procter, D.M. Martin, M. Clamp, G.J. Barton, Jalview Version 2—a multiple sequence alignment editor and analysis workbench, Bioinformatics. 25 (2009) 1189–1191.

[23] W. Humphrey, A. Dalke, K. Schulten, VMD: visual molecular dynamics, J. Mol. Graph. 14 (33–8) (1996) 27–28.

[24] S.B. delCardayre, K.P. Stock, G.L. Newton, R.C. Fahey, J.E. Davies, Coenzyme A disulfide reductase, the primary low molecular weight disulfide reductase from Staphylococcus aureus. Purification and characterization of the native enzyme, J. Biol. Chem. 273 (1998) 5744–5751.

[25] N.R. Yun, K.Y. San, G.N. Bennett, Enhancement of lactate and succinate formation in adhE or pta-ackA mutants of NADH dehydrogenase-deficient Escherichia coli, J. Appl. Microbiol. 99 (2005) 1404–1412.

[26] L.A. Schurig-Briccio, T. Yano, H. Rubin, R.B. Gennis, Characterization of the type 2 NADH:menaquinone oxidoreductases from Staphylococcus aureus and the bactericidal action of phenothiazines, Biochim. Biophys. Acta 1837 (2014) 954–963.

[27] W. Kabsch, Automatic processing of rotation diffraction data from crystals of initially unknown symmetry and cell constants, J. Appl. Crystallogr. 26 (1993) 795–800.

[28] S. Bailey, The Ccp4 suite - programs for protein crystallography, Acta Crystallogr. D. 50 (1994) 760–763.

[29] H.M. Berman, J. Westbrook, Z. Feng, G. Gilliland, T.N. Bhat, H. Weissig, I.N. Shindyalov, P.E. Bourne, The protein data bank, Nucleic Acids Res. 28 (2000) 235–242.

[30] M.D. Warner, V. Lukose, K.H. Lee, K. Lopez, M.H. Sazinsky, E.J. Crane, Characterization of an NADH-dependent persulfide reductase from Shewanella loihica PV-4: implications for the mechanism of sulfur respiration via FAD-dependent enzymes, Biochemistry. 50 (2011) 194–206.

[31] L.A. Kelley, S. Mezulis, C.M. Yates, M.N. Wass, M.J. Sternberg, The Phyre2 web portal for protein modeling, prediction and analysis, Nat. Protoc. 10 (2015) 845–858.

[32] P.D. Adams, P.V. Afonine, G. Bunkoczi, V.B. Chen, I.W. Davis, N. Echols, J.J. Headd, L.W. Hung, G.J. Kapral, R.W. Grosse-Kunstleve, A.J. McCoy, N.W. Moriarty, R. Oeffner, R.J. Read, D.C. Richardson, J.S. Richardson, T.C. Terwilliger, P.H. Zwart, PHENIX: a comprehensive Python-based system for macromolecular structure solution, Acta Crystallogr. D Biol. Crystallogr. 66 (2010) 213–221.

[33] B.W. Matthews, Solvent content of protein crystals, J. Mol. Biol. 33 (1968) 491–497.

[34] P. Emsley, K. Cowtan, Coot: model-building tools for molecular graphics, Acta Crystallogr. D Biol. Crystallogr. 60 (2004) 2126–2132.

[35] M.G. Rossmann, D. Moras, K.W. Olsen, Chemical and biological evolution of nucleotide-binding protein, Nature. 250 (1974) 194–199.

[36] Y. Feng, W. Li, J. Li, J. Wang, J. Ge, D. Xu, Y. Liu, K. Wu, Q. Zeng, J.W. Wu, C. Tian, B. Zhou, M. Yang, Structural insight into the type-II mitochondrial NADH dehydrogenases, Nature. 491 (2012) 478–482.

[37] A. Argyrou, J.S. Blanchard, Flavoprotein disulfide reductases: advances in chemistry and function, Prog. Nucleic Acid Res. Mol. Biol. 78 (2004) 89–142.

[38] A.M. Lencina, Z. Ding, L.A. Schurig-Briccio, R.B. Gennis, Characterization of the Type III sulfide:quinone oxidoreductase from Caldivirga maquilingensis and its membrane binding, Biochim. Biophys. Acta 1827 (2013) 266–275.

[39] G.L. Ellman, Tissue sulfhydryl groups, Arch. Biochem. Biophys. 82 (1959) 70–77.

[40] Sea, K., Lee, J., To, D., Chen, B., Sazinsky, M. H. & Crane, E. J., 3rd (2018) A broader active site in Pyrococcus horikoshii CoA disulfide reductase accommodates larger substrates and reveals evidence of subunit asymmetry, FEBS Open Bio. 8, 1083–1092.

[41] J.A. Boylan, C.S. Hummel, S. Benoit, J. Garcia-Lara, J. Treglown-Downey, E.J. Crane 3rd, F.C. Gherardini, Borrelia burgdorferi bb0728 encodes a coenzyme A disulphide reductase whose function suggests a role in intracellular redox and the oxidative stress response, Mol. Microbiol. 59 (2006) 475–486.

[42] N. Bernard, K. Johnsen, J.J. Holbrook, J. Delcour, D175 discriminates between NADH and NADPH in the coenzyme binding site of Lactobacillus delbrueckii subsp. bulgaricus D-lactate dehydrogenase, Biochem. Biophys. Res. Commun. 208 (1995) 895–900.

[43] B.D. Wallace, J.S. Edwards, J.R. Wallen, W.J. Moolman, R. van der Westhuyzen, E. Strauss, M.R. Redinbo, A. Claiborne, Turnover-dependent covalent inactivation of Staphylococcus aureus coenzyme A-disulfide reductase by coenzyme A-mimetics: mechanistic and structural insights, Biochemistry. 51 (2012) 7699–7711.

[44] T.C. Mallett, J.R. Wallen, P.A. Karplus, H. Sakai, T. Tsukihara, A. Claiborne, Structure of coenzyme A-disulfide reductase from Staphylococcus aureus at 1.54 A resolution, Biochemistry. 45 (2006) 11278–11289.

[45] M.S. Patel, N.S. Nemeria, W. Furey, F. Jordan, The pyruvate dehydrogenase complexes: structure-based function and regulation, J. Biol. Chem. 289 (2014) 16615–16623.

[46] M. Iwata, Y. Lee, T. Yamashita, T. Yagi, S. Iwata, A.D. Cameron, M.J. Maher, The structure of the yeast NADH dehydrogenase (Ndi1) reveals overlapping binding sites for water- and lipid-soluble substrates, Proc. Natl. Acad. Sci. U. S. A. 109 (2012) 15247–15252.

[47] A. Heikal, Y. Nakatani, E. Dunn, M.R. Weimar, C.L. Day, E.N. Baker, J.S. Lott, L.A. Sazanov, G.M. Cook, Structure of the bacterial type II NADH dehydrogenase: a monotopic membrane protein with an essential role in energy generation, Mol. Microbiol. 91 (2014) 950–964.